

Highly sensitive, multi-stage, and mid-infrared refractive index sensor based on photonic spin Hall effect

Jiaye Ding(丁嘉烨), Chenglong Wang(汪承龙), Shengli Liu(刘胜利), Peng Dong(董鹏), and Jie Cheng(程杰)
Citation: Chin. Phys. B, 2026, 35 (**1**): 014201. DOI: 10.1088/1674-1056/ade24c
http://cpb.iphy.ac.cn; http://iopscience.iop.org/cpb

What follows is a list of articles you may be interested in

Surface phonon resonance: A new mechanism for enhancing photonic spin Hall effect and refractive index sensor

Jie Cheng(程杰), Chenglong Wang(汪承龙), Yiming Li(李一铭), Yalin Zhang(张亚林), Shengli Liu(刘胜利), and Peng Dong(董鹏)
Chin. Phys. B, 2024, 33 (**8**): 084201. DOI: 10.1088/1674-1056/ad4a3c

Multi-functional photonic spin Hall effect sensor controlled by phase transition

Jie Cheng(程杰), Rui-Zhao Li(李瑞昭), Cheng Cheng(程骋), Ya-Lin Zhang(张亚林), Sheng-Li Liu(刘胜利), and Peng Dong(董鹏)
Chin. Phys. B, 2024, 33 (**7**): 074203. DOI: 10.1088/1674-1056/ad3b85

Engineered photonic spin Hall effect of Gaussian beam in antisymmetric parity-time metamaterials

Lu-Yao Liu(刘露遥), Zhen-Xiao Feng(冯振校), Dong-Mei Deng(邓冬梅), and Guang-Hui Wang(王光辉)
Chin. Phys. B, 2023, 32 (**9**): 094201. DOI: 10.1088/1674-1056/accb89

Numerical simulation of a truncated cladding negative curvature fiber sensor based on the surface plasmon resonance effect

Zhichao Zhang(张志超), Jinhui Yuan(苑金辉), Shi Qiu(邱石), Guiyao Zhou(周桂耀), Xian Zhou(周娴), Binbin Yan(颜玢玢), Qiang Wu(吴强), Kuiru Wang(王葵如), and Xinzhu Sang(桑新柱)
Chin. Phys. B, 2023, 32 (**3**): 034208. DOI: 10.1088/1674-1056/ac785e

A theoretical study of a plasmonic sensor comprising a gold nano-disk array on gold film with a SiO_2 spacer

Xiangxian Wang(王向贤), Jiankai Zhu(朱剑凯), Huan Tong(童欢), Xudong Yang(杨旭东), Xiaoxiong Wu(吴枭雄), Zhiyuan Pang(庞志远), Hua Yang(杨华), Yunping Qi(祁云平)
Chin. Phys. B, 2019, 28 (**4**): 044201. DOI: 10.1088/1674-1056/28/4/044201

Highly sensitive, multi-stage, and mid-infrared refractive index sensor based on photonic spin Hall effect

Jiaye Ding(丁嘉烨)[1,†], Chenglong Wang(汪承龙)[1,2,†], Shengli Liu(刘胜利)[1], Peng Dong(董鹏)[3,‡], and Jie Cheng(程杰)[1,§]

[1] *School of Science, Jiangsu Province Engineering Research Center of Low Dimensional Physics and New Energy, Nanjing University of Posts and Telecommunications, Nanjing* 210023, *China*

[2] *College of Electronic and Optical Engineering & College of Flexible Electronics (Future Technology), Nanjing University of Posts and Telecommunications, Nanjing* 210023, *China*

[3] *College of Electronic Information Engineering & College of Integrated Circuits, Research Center of Intelligent Sensor and Network Engineering Technology of Jiangsu Province, Nanjing University of Industry Technology, Nanjing* 210023, *China*

(Received 8 April 2025; revised manuscript received 29 May 2025; accepted manuscript online 9 June 2025)

Surface polaritons, as surface electromagnetic waves propagating along the surface of a medium, have played a crucial role in enhancing photonic spin Hall effect (PSHE) and developing highly sensitive refractive index (RI) sensors. Among them, the traditional surface plasmon polariton (SPP) based on noble metals limits its application beyond the near-infrared (IR) regime due to the large negative permittivity and optical losses. In this contribution, we theoretically proposed a highly sensitive PSHE sensor with the structure of Ge prism-SiC-Si:InAs-sensing medium, by taking advantage of the hybrid surface plasmon phonon polariton (SPPhP) in mid-IR regime. Here, heavily Si-doped InAs (Si:InAs) and SiC excite the SPP and surface phonon polariton (SPhP), and the hybrid SPPhP is realized in this system. More importantly, the designed PSHE sensor based on this SPPhP mechanism achieves the multi-stage RI measurements from 1.00025–1.00225 to 1.70025–1.70225, and the maximal intensity sensitivity and angle sensitivity can be up to 9.4×10^4 μm/RIU and 245 °/RIU, respectively. These findings provide a new pathway for the enhancement of PSHE in mid-IR regime, and offer new opportunities to develop highly sensitive RI sensors in multi-scenario applications, such as harmful gas monitoring and biosensing.

Keywords: refractive index (RI) sensor, photonic spin Hall effect, mid-IR, multi-stage

PACS: 42.25.–p, 41.20.Jb, 42.79.–e, 78.20.Ci

DOI: 10.1088/1674-1056/ade24c **CSTR:** 32038.14.CPB.ade24c

1. Introduction

As an optical version of the electronic spin Hall effect, the photonic spin Hall effect (PSHE) has attracted much attention since it was first discovered by Hosten and Kwiat's group in 2008.[1] Here, the spin photons and refractive index gradient in PSHE play the analogous roles of the spin electrons and potential gradient, respectively. The PSHE manifesting itself as spin-dependent lateral displacement and splitting of the left- and right-handed circularly polarized components, can be considered as a result of the spin–orbit interaction of light.[2] Owing to its unique physical connotation, the PSHE holds potential applications in many fields, including quantum weak measurement, image edge detection, and precision metrology.[3–5]

In view of the intimate relationship between transverse spin shifts and interface variations, the PSHE has been widely used to monitor the tiny changes in physical parameters.[6,7] As a fundamental quantity to characterize the optical property of a system, the accurate measurement of refractive index (RI) is of great significance. More precisely, extremely small variation in RI can make a huge difference in the spin shifts of PSHE.[8,9] Therefore, the PSHE can be regarded as a key leading indicator to RI changes, which provides an effective metrological tool and a new platform for RI sensing. In contrast to other traditional RI sensors, the PSHE sensing shows obvious superiority in terms of high sensitivity, desirable accuracy, and high signal-to-noise ratio.[10] For example, the PSHE sensor can discriminate the gastric normal and cancer cells with an excellent sensitivity of 6.1×10^5 μm/RIU, about four orders of magnitude greater than pervious reported resonant optical tunneling effect sensor.[11] Among them, the most well-exploited technique for PSHE sensor is based on the surface plasmon polariton (SPP) in visible and near-infrared (IR) regions.[12–14] However, the noble metals (like gold and silver), as traditional plasmon materials, have very large negative permittivity and inherent optical losses in longer wavelengths, restricting its usefulness of SPP beyond the near-IR.[15]

Similar to the visible and near-IR regions, mid-IR is an extremely significant wavelength range for various sensing

[†]These authors contributed equally to this work.

[‡]Corresponding author. E-mail: 2021101298@niit.edu.cn

[§]Corresponding author. E-mail: chengj@njupt.edu.cn

© 2026 Chinese Physical Society and IOP Publishing Ltd. All rights, including for text and data mining, AI training, and similar technologies, are reserved.

applications, due to the fact that many essential molecules have the absorption bands in this wavelength regime.[16] It is highly desirable to look for other alternatives to metals that can achieve the mid-IR plasmonics. A perfect candidate for this purpose is doped semiconductors, because of their promising advantages of lower optical losses, active manipulation of carrier concentration, and drastic modulation of plasmonic properties via doping.[17] Similarly to SPP, surface phonon polariton (SPhP) is also one of the well-known surface polaritons, which results from the interaction between photons and phonons of polar dielectric materials (such as SiC).[18] Note that the reports on SPhP-enhanced PSHE and corresponding sensing mechanism have been recently put forward.[19] In particular, both SPP and SPhP can be excited by the p-polarized light with typical Kretschmann–Raether configuration in the same mid-IR range.[20,21] This fact thus naturally raises a question: can we construct a structure to generate the SPP and SPhP simultaneously, and whether the PSHE can be enhanced by the hybrid of SPP and SPhP (abbreviation for SPPhP). It has been demonstrated that the hybrid surface plasmon–exciton polariton (SPEP) system exhibits enhanced RI sensing performance (e.g., higher detection sensitivity) when compared to the respective SPP and surface exciton polariton (SEP) sensors.[22] Consequently, we are curious to investigate whether the PSHE sensor based on SPPhP mechanism presents superior sensitivity to that of single SPP system in mid-IR regime.

In this work, the SPP structure containing heavily Si-doped InAs is proposed, however, the RI detection sensitivity is not very good. In order to fulfill application requirements and enhance the sensing performance, we introduce the phonon SiC layer into the original SPP system, which can realize the hybrid of SPP and SPhP. Moreover, the PSHE sensor based on this SPPhP mechanism displays excellent sensitivity for the multi-stage RI measurements. These findings offer new opportunities in multi-scenario detection, such as harmful gas monitoring and biosensing.

2. Theory and model

According to the generation of traditional SPP in noble metals, the SPP in mid-IR regime can also be excited by a typical Kretschmann–Raether configuration, where the metal film is replaced by the doped semiconductor, as illustrated in Fig. 1(a). Here, heavily Si:InAs is selected as the mid-IR plasmon material, and its dielectric constant can be expressed by Drude model[17]

$$\varepsilon_{\mathrm{si:InAs}}(\omega)=\varepsilon'_{\mathrm{si:InAs}}+\mathrm{i}\varepsilon''_{\mathrm{si:InAs}}=\varepsilon_{\mathrm{s}}\left(1-\frac{\omega_{\mathrm{p}}^2}{\omega^2+\mathrm{i}\Gamma\omega}\right),$$
$$\omega_{\mathrm{p}}^2=\frac{ne^2}{\varepsilon_{\mathrm{s}}\varepsilon_0 m^*}, \tag{1}$$

where Γ is the scattering rate of carriers in the semiconductor. ω_{p} is the plasma frequency of the doped material, which can be determined by the effective mass m^*, the concentration n of the free carriers in the semiconductor, the electron charge e, the free space dielectric constant ε_0, and the relative dielectric constant ε_{s} (12.04) of the undoped semiconductor, respectively. The relationship between the dielectric constant of Si:InAs and the wavelength of incident light is plotted in Fig. 1(b). It can be clearly seen that when the wavelength of incident light is greater than about 9 μm, that is, the cyan region in Fig. 1(b), the permittivity of Si:InAs displays a negative real part, indicating the excitation of SPP. In order to satisfy the requirements for surface plasmon resonance (SPR), the Si:InAs film is deposited over a high RI prism of Ge. The use of Ge prism in this work also has the following advantages: (i) large spectral transparency window from 2 μm to 15 μm, covering the whole molecule fingerprint; (ii) its high RI allows the implementation of devices with reduced footprint.[23] The RI of Ge prism is given by[24]

$$n_{\mathrm{Ge}}=\sqrt{9.28156+\frac{6.7288\lambda^2}{\lambda^2-0.44105}+\frac{0.21307\lambda^2}{\lambda^2-3870.1}}, \tag{2}$$

where the unit of λ in the formula is micron.

To construct the system of hybrid SPP and SPhP, the phonon material SiC is introduced into the original SPP structure (shown in Fig. 1(c)). Analogous to the above Si:InAs, the frequency-dependent dielectric constant of SiC can be described by the Drude–Lorentz model[25]

$$\varepsilon_{\mathrm{SiC}}(\omega)=\varepsilon'_{\mathrm{SiC}}+\mathrm{i}\varepsilon''_{\mathrm{SiC}}=\varepsilon_\infty\frac{\omega^2-\omega_{\mathrm{LO}}^2+\mathrm{i}\gamma\omega}{\omega^2-\omega_{\mathrm{TO}}^2+\mathrm{i}\gamma\omega}, \tag{3}$$

where the longitudinal and transverse optical phonon frequencies are $\omega_{\mathrm{LO}}=972\ \mathrm{cm}^{-1}$ and $\omega_{\mathrm{TO}}=796\ \mathrm{cm}^{-1}$, respectively. The damping rate is due to vibrational anharmonicity with the value of $\gamma=3.75\ \mathrm{cm}^{-1}$, and the high-frequency dielectric constant is $\varepsilon_\infty=6.5$. The Reststrahlen band of SiC defined by $\varepsilon'_{\mathrm{SiC}}<0$ (10.3 μm–12.5 μm, cyan region in Fig. 1(d)) corresponds to the wavelength regime for exciting SPhP, which is highly overlapped with the SPP excitation wavelength (> 9 μm) for Si:InAs.

A linearly polarized Gaussian beam is incident into the SPP and SPPhP structures, and the PSHE of reflected light appears in the y-axis direction. The angular spectrum of incident light can be written as[26]

$$\tilde{E}_{\mathrm{i}\pm}=(e_{\mathrm{i}x}\pm e_{\mathrm{i}y})\frac{w_0}{\sqrt{2\pi}}\exp\left[-\frac{(k_{\mathrm{i}x}^2+k_{\mathrm{i}y}^2)\omega_0^2}{4}\right], \tag{4}$$

in which $w_0=0.5$ mm is the beam waist. Using the transfer matrix and boundary continuity condition, we can obtain the quantitative relationship between the incident and reflected

fields[26]

$$\begin{bmatrix} \tilde{E}_{\mathrm{r}}^{\mathrm{H}} \\ \tilde{E}_{\mathrm{r}}^{\mathrm{V}} \end{bmatrix} = \begin{bmatrix} r_{\mathrm{p}} & \dfrac{k_{\mathrm{ry}} \cot\theta_{\mathrm{i}} (r_{\mathrm{p}} + r_{\mathrm{s}})}{k_0} \\ \dfrac{-k_{\mathrm{ry}} \cot\theta_{\mathrm{i}} (r_{\mathrm{p}} + r_{\mathrm{s}})}{k_0} & r_{\mathrm{s}} \end{bmatrix} \begin{bmatrix} \tilde{E}_{\mathrm{i}}^{\mathrm{H}} \\ \tilde{E}_{\mathrm{i}}^{\mathrm{V}} \end{bmatrix}. \quad (5)$$

Here, k_0 is the wave number in free space. H and V represent horizontal and vertical polarization, respectively. Then, the transverse spin shift can be expressed as[27]

$$\delta_{\mathrm{H}}^{\pm} = \mp \frac{k_0 w_0^2 \mathrm{Re}(1 + r_{\mathrm{s}}/r_{\mathrm{p}}) \cot\theta_{\mathrm{i}}}{k_0^2 w_0^2 + \left|\frac{\partial \ln r_{\mathrm{p}}}{\partial \theta_{\mathrm{i}}}\right|^2 + \left|(1 + r_{\mathrm{s}}/r_{\mathrm{p}}) \cot\theta_{\mathrm{i}}\right|^2}, \quad (6)$$

$$\delta_{\mathrm{V}}^{\pm} = \mp \frac{k_0 w_0^2 \mathrm{Re}(1 + r_{\mathrm{p}}/r_{\mathrm{s}}) \cot\theta_{\mathrm{i}}}{k_0^2 w_0^2 + \left|\frac{\partial \ln r_{\mathrm{s}}}{\partial \theta_{\mathrm{i}}}\right|^2 + \left|(1 + r_{\mathrm{p}}/r_{\mathrm{s}}) \cot\theta_{\mathrm{i}}\right|^2}. \quad (7)$$

Here $r_{\mathrm{p,s}} = |r_{\mathrm{p,s}}| \exp(\mathrm{i}\varphi_{\mathrm{p,s}})$ are the Fresnel reflection coefficients of p- and s-polarized waves.

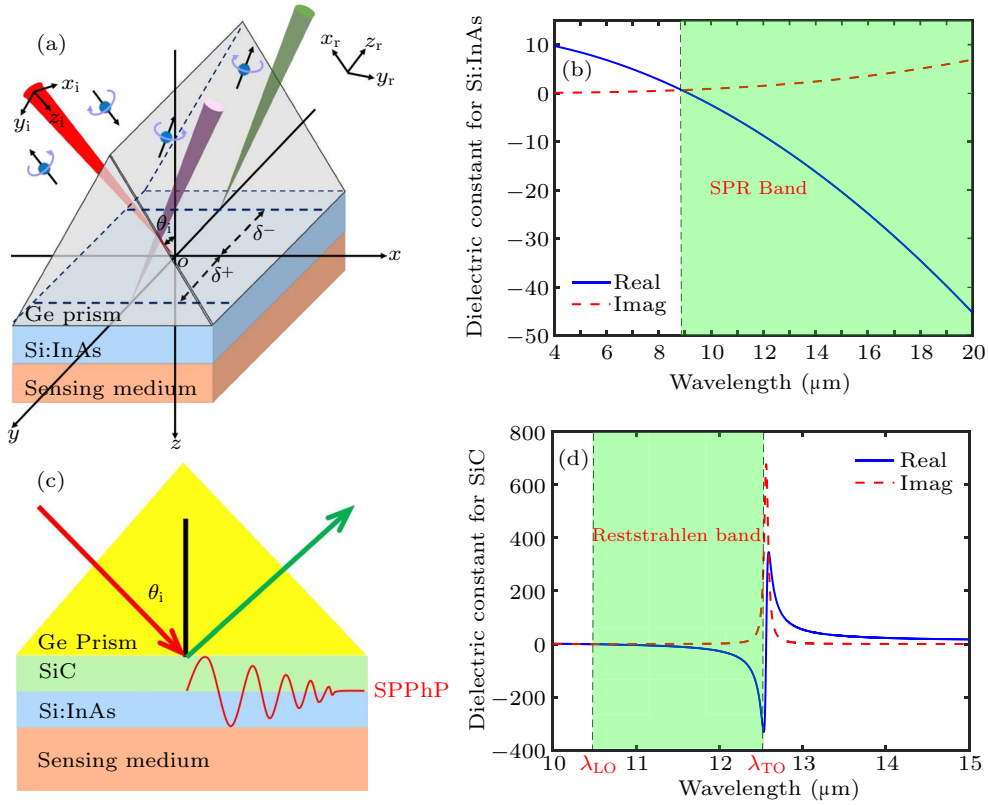


Fig. 1. (a) and (c) Schematic illustration of PSHE in the SPP and SPPhP structures consisting of Ge prism, Si:InAs, SiC, and sensing medium. (b) and (d) The dielectric constants for Si:InAs and SiC.

3. Results and analysis

Firstly, we investigate the PSHE and corresponding sensing performance for the SPP structure of Ge prism-Si:InAs-sensing medium (in Fig. 1(a)). The wavelength of incident light is fixed to 10.4 μm (within the mid-IR range), and we set the RI of sensing medium to be 1 (i.e., air). To demonstrate the excitation of SPP in this structure, Fresnel reflection coefficients $|r_{\mathrm{p,s}}|$ as a function of incident angle is shown in Fig. 2(a). Obviously, $|r_{\mathrm{s}}|$ varies monotonically with the increase of incident angle, while there is a narrow dip (~ 0.054) at 16.35° in the $|r_{\mathrm{p}}|$ reflection curve, due to the remarkable SPR effect of Si:InAs-based configuration in the mid-IR region. As displayed in the inset of Fig. 2(b), this dip of $|r_{\mathrm{p}}|$ can lead to an observable value (~ 4) of Fresnel coefficient ratio $|r_{\mathrm{s}}/r_{\mathrm{p}}|$. Considering the intimate relationship between the PSHE and $|r_{\mathrm{s}}/r_{\mathrm{p}}|$,[5,10,12] the transverse displacement δ_{H} of Ge prism-Si:InAs-air presents a distinct peak around the resonance angle of 16.35°. However, the maximum value of δ_{H} under the optimal thickness of Si:InAs layer is relatively small, only about 1.5 times the wavelength of incident light, which is mainly owing to the tiny value of $|r_{\mathrm{s}}/r_{\mathrm{p}}|$.

Monitoring the transverse displacement of PSHE is demonstrated to be an effective and innovative technology to detect tiny RI variations of sensing medium.[10] Thus, we will discuss the application of this Si:InAs-based structure in PSHE sensor, and the corresponding detection performance can be generally evaluated by both the intensity and angle sensitivity. The intensity sensitivity can be defined as $S_\delta = \Delta\delta/\Delta n_{\mathrm{s}}$, where $\Delta\delta$ is the difference of transverse displacement (under a fixed incident angle) caused by an RI change Δn_{s} of sensing medium.[5] Similarly, $S_\theta = \Delta\theta/\Delta n_{\mathrm{s}}$ is used to describe the angle sensitivity, in which $\Delta\theta$ is the variation of incident angle, corresponding to the peak/valley of transverse displacement. Figure 2(c) shows the changes of transverse displacement δ_{H}

with the different RI values of sensing medium. We find that the PSHE is very sensitive to the RI variation (1.00025–1.00225), and by fixing the incident angle of 16.35°, the transverse displacement changes from 15.61 μm to 15.9 μm. In addition, the resonance angle corresponding to maximal δ_H increases from 16.31° to 16.35°. The transverse displacement and resonance angle versus the RI of sensing medium are plotted in Figs. 2(d) and 2(e), which basically presents a linear relation. To describe the sensing performance more clearly, the linear fitting method is adopted, and then, the intensity and angle sensitivity of 135 μm/RIU and 20 °/RIU are obtained. R^2 is usually used to evaluate the quality of the linear fitting, here R^2 are 0.98 and 1 for fitting the intensity and angle sensitivity, respectively, which indicates that the RI detection of PSHE sensor based on Si:InAs structure is quite reliable. Unfortunately, such detection performance for the RI range 1.00025–1.00225 cannot meet the sensitivity requirements in practical sensing application.

With the rapid development of high-precision measurements, new demands have been put forward for the multi-functional and multi-scenario detection of sensor.[28–30] Therefore, the detection in various RI sensing ranges is performed by the above Si:InAs-based PSHE structure. Here, we take the multi-stage RI detection of 1.00025–1.00225 to 1.70025–1.70225 as examples. For simplicity, the RI range 1.00025–1.00225 is denoted as n_s1, and 1.70025–1.70225 can be numbered as n_s8 in sequence. Table 1 displays the detection sensitivity of this Si:InAs-based PSHE sensor in various RI ranges. It is obvious that, when we increase the RI of sensing medium, the sensing performance shows a noticeable improvement. For the RI detection range of 1.70025–1.70225, the intensity and angle sensitivity can be enhanced to 3600 μm/RIU and 50 °/RIU, respectively. In order to the better practical application, further enhancement in sensing performance is highly desirable.

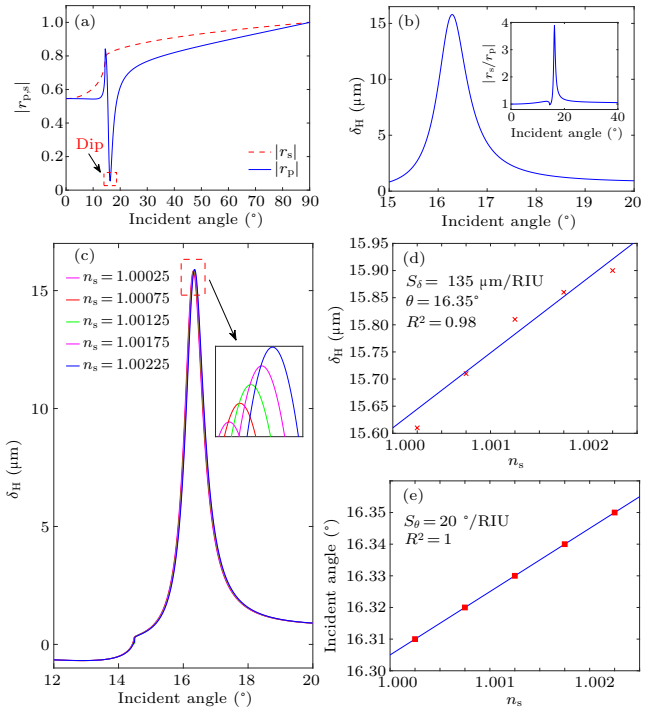


Fig. 2. (a)–(b) Fresnel reflection coefficients $|r_{p,s}|$ and transverse displacements δ_H as a function of incident angle in the SPP structure of Ge prism-Si:InAs-air. The ratio $|r_s/r_p|$ is shown in the inset of panel (b). (c)–(e) Description of intensity and angle sensitivity for PSHE sensor based on SPP structure.

Table 1. Detection performance of Si:InAs-based PSHE sensor in the multiple RI ranges.

RI sensing range	Fixed incident angle (°)	Intensity sensitivity (μm/RIU)	Angle sensitivity (°/RIU)
n_s1:[1.00025–1.00225]	16.35	135	20
n_s2:[1.10025–1.10225]	18.59	255	20
n_s3:[1.20025–1.20225]	21.03	395	25
n_s4:[1.30025–1.30225]	23.7	630	30
n_s5:[1.40025–1.40225]	26.61	860	35
n_s6:[1.50025–1.50225]	29.76	1540	40
n_s7:[1.60025–1.60225]	33.27	2535	45
n_s8:[1.70025–1.70225]	36.97	3600	50

Surface polaritons, as the surface electromagnetic waves propagating along a surface of a medium, can be classified into three different types: SPP, SEP, and SPhP.[31] Previous investigations have demonstrated that all these three polaritons make great contributions to the enhancement of PSHE.[14,19,32] Very recently, the sensing mechanism based on hybrid polariton is reported, which can significantly improve the transverse displacements and detection performance.[22,33,34] For the mid-IR regime in this work, in order to further enhance the sensing performance, we introduce the SiC layer (phonon material) into above Si:InAs-based SPP structure, and then a structural configuration of Ge prism-SiC-Si:InAs-sensing medium (in Fig. 1(c)) can be established. Given that the wavelength requirements of Si:InAs and SiC to excite SPP and SPhP are > 9 μm and 10.3 μm–12.5 μm, respectively, the wavelength of incident light is still set to be 10.4 μm in the following calculations. Figure 3(a) shows the Fresnel reflection coefficients $|r_{p,s}|$ versus incident angle for the Ge prism-SiC-Si:InAs-air structure. A similar dip occurs in the Fresnel reflection coefficient of p-polarized beam, and the minimal value of $|r_p|$ is

about 0.00013 at 22.65°, which is much smaller than that of Si:InAs-based SPP structure, demonstrating the strong excitation of hybrid SPPhP. As a result, we obtain a large value of $|r_s/r_p|$, and as exhibited in Fig. 3(b), the maximal transverse displacement can be up to 15 times incident wavelength. As compared with the case of Si:InAs-based SPP structure, the transverse displacement is promoted by 10 times with the addition of SiC layer. Therefore, the hybrid SPPhP structure of Ge prism-SiC-Si:InAs-air represents the significant enhancement of PSHE, and the subsequent sensing performance is highly anticipated.

To further elucidate the underlying physical mechanism of this giant transverse displacements based on SPPhP, we introduce the concepts of normal mode (spin maintenance without geometric phase) and abnormal mode (spin reflection with geometric phase).[35] Here, the internal spin components of the reflected beam can be regarded as the combination of normal and abnormal modes corresponding to different helicities. The reflection coefficient for the normal (r_{normal}) and the abnormal (r_{abnormal}) modes can be expressed as follows:[35] $r_{\text{normal}} = (r_p + r_s)/2$, $r_{\text{abnormal}} = (r_p - r_s)/2$. As illustrated in Fig. 3(c), the opposite sign (i.e., $r_{\text{normal}} = -r_{\text{abnormal}}$) occurs at the resonance angle of 22.56°, thereby destructive interference between such modes leads to the vanishing of the reflection of the p-polarized incidence and then a significant PSHE.

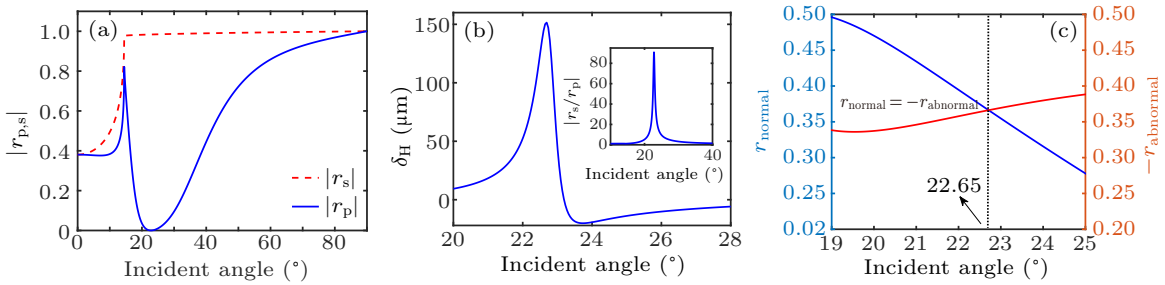


Fig. 3. (a) Fresnel reflection coefficients $|r_{p,s}|$, (b) transverse displacements δ_H, and (c) variation of Fresnel coefficients (r_{normal}, $-r_{\text{abnormal}}$) as a function of incident angle in the SPPhP structure of Ge prism-SiC-Si:InAs-air.

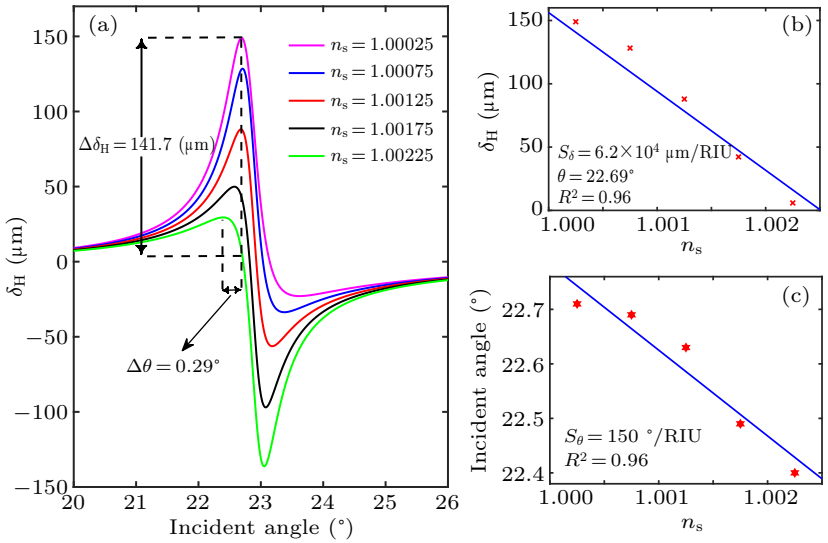


Fig. 4. The intensity and angle sensitivity for PSHE sensor based on the hybrid SPPhP structure of Ge prism-SiC-Si:InAs-sensing medium.

For PSHE sensor based on the hybrid structure of Ge prism-SiC-Si:InAs-sensing medium, the transverse displacement for detecting different analytes with the RI range of 1.00025–1.00225 is displayed in Fig. 4(a). By increasing the RI of sensing medium, there is an apparent drop in the peak of transverse displacement, moreover, the incident angle corresponding to the peak moves towards a smaller angle. More specifically, the transverse displacement undergoes a significant difference $\Delta\delta$ of 141.7 μm when the incident angle is fixed at 22.69°. The incident angle corresponding to the peak of transverse displacement varies from 22.69° to 22.40°, with the decreased $\Delta\theta$ of 0.29°. Combined with the linear fitting method in Figs. 4(b) and 4(c), the intensity sensitivity of 6.2×10^4 μm/RIU and angle sensitivity of 150 °/RIU are obtained easily. Both R^2 values are 0.96, further indicating the reliability of linear fitting results. In comparison with the result of Si:InAs-based SPP structure, the intensity sensitivity of PSHE sensor with the additional SiC layer is enhanced two orders of magnitude, accompanied by sevenfold improvement in angle sensitivity. Therefore, the additive phonon SiC layer

and then relevant excitation of hybrid SPPhP play a vital role in the great enhancement of sensing performance.

In order to verify whether the hybrid SPPhP structure of Ge prism-SiC-Si:InAs-sensing medium can exhibit the outstanding detection performance in various application fields, figure 5 shows both the intensity and angle sensitivity in the multi-stage RI detections. Here, the measured RI range of n_s1 to n_s8 is previously illustrated in Table 1. The sensing performance is excellent for all the multi-stage RI measurements, and the maximal intensity and angle sensitivity can reach 9.4×10^4 μm/RIU and 245 °/RIU, respectively. Table 2 displays a comparison of detection performance between our proposed structure and PSHE sensors based on other surface polaritons. From Table 2, the intensity (angle) sensitivity for PSHE sensors based on single surface polaritons (i.e., SPP, SEP, and SPhP) are 6.60×10^3 μm/RIU (108 °/RIU),[14] 6.32×10^3 μm/RIU (88 °/RIU),[32] and 9.07×10^4 μm/RIU (237 °/RIU).[19] Previous report shows that the detection sensitivity for the hybrid SPEP structure is 2.08×10^5 μm/RIU and 211 °/RIU, respectively.[22] In this contribution, the intensity sensitivity of our hybrid SPPhP structure is close to 10^5 μm/RIU; meanwhile, the angle sensitivity can be up to 245 °/RIU. These detection sensitivities can rival with those of hybrid SPEP sensor, indicating the superior sensing performance. More importantly, the proposed SPPhP sensor can realize the multi-stage RI measurements with both high intensity and angle sensitivity, which demonstrates the application potential in multi-scenario sensing and detection. For example, the RI value of harmful gas (such as NO_2) is within the n_s1 range,[19] while the waterborne bacteria and cancer cells are located in the RI regions of 1.365–1.422, and 1.659–1.662, respectively.[11,29] Therefore, the proposed PSHE sensor based on hybrid SPPhP structure is very promising in many application fields, including the harmful gas monitoring and biosensing.

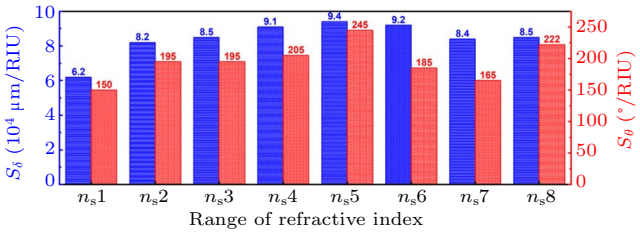


Fig. 5. The intensity and angle sensitivity of the hybrid SPPhP sensor for the multi-stage RI measurement.

Table 2. Comparison of our proposed hybrid SPPhP sensor with PSHE sensors based on other surface polaritons.

Mechanism	Measured RI range	Muti-stage detection	Intensity sensitivity (μm/RIU)	Angle sensitivity (°/RIU)	Reference
SPP	1.458–1.459	no	6.60×10^3	108	[14]
SEP	1.00027821–1.00095981	no	6.32×10^3	88	[32]
SPhP	1.00027–1.00107	no	9.07×10^4	237	[19]
SPEP	1.000–1.001	no	2.08×10^5	211	[22]
SPPhP	1.00025–1.70225	yes	9.4×10^4	245	this work

Note that, this work focuses on the theoretical validation; nevertheless we would like to elaborate on the feasibility of the experimental verification for this sensor. The designed PSHE sensor is composed of four layers: Ge prism, SiC, Si:InAs, and sensing medium. These materials are very common; therefore, the proposed sensor is simple in structure and easy to fabricate. For example, the Si:InAs films with doping densities ranging from 2.7×10^{18} cm^{-3} to 7.5×10^{19} cm^{-3} are successfully grown by molecular beam epitaxy in 2012, and its plasma frequency can be controlled across a broad range of mid-IR frequencies.[17] This study also demonstrates that, the accurate and reproducible control of plasmonic structures' optical properties with nanometer-scale accuracy is achievable.[17] In addition, the experimental observation of spin shift for PSHE can be based on the weak measurement method, in which a preselection and postselection technique are adopted to enhance the original shift by nearly four orders of magnitude.[1] These above reports have laid the strong foundation for the experimental verification of our proposed PSHE sensor.

4. Conclusions

In summary, we theoretically proposed a highly sensitive and mid-IR PSHE sensor, which presents the multi-stage RI measurements and holds great potential in multi-scenario detections. Firstly, we established an SPP structure of Ge prism-Si:InAs-sensing medium. The transverse displacement of PSHE in this system is very sensitive to the tiny RI change; however, the detection sensitivity is not very high. Then, we introduced the phonon SiC layer into original SPP system, and the hybrid SPPhP structure of Ge prism-SiC-Si:InAs-sensing medium was accordingly constructed. The maximal transverse displacement is about 10 times greater than that of the origin SPP system. Moreover, PSHE sensor based on this SPPhP mechanism displays excellent sensing performance in the multi-stage RI detections from 1.00025–1.00225 to 1.70025–1.70225, and as perfect as the hybrid SPEP sensor, its maximal intensity and angle sensitivity can be up to 9.4×10^4 μm/RIU and 245 °/RIU, respectively. These results demonstrate the significant contribution of hybrid SPPhP to

the enhanced PSHE in mid-IR regime, and provide an opportunity to develop highly sensitive PSHE sensors for multi-scenario detections, such as the harmful gas monitoring and biosensing.

Acknowledgements

Project supported by the National Natural Science Foundation of China (Grant No. 12175107), the Qing Lan Project of Jiangsu Province, the Hua Li Talents Program of Nanjing University of Posts and Telecommunications, Natural Science Foundation of Nanjing Vocational University of Industry Technology (Grant No. YK22-02-08), and the Fund from the Research Center of Industrial Perception and Intelligent Manufacturing Equipment Engineering of Jiangsu Province, China (Grant No. ZK21-05-09).

References

[1] Hosten O and Kwiat P 2008 *Science* **319** 787
[2] Bliokh K Y and Bliokh Y P 2006 *Phys. Rev. Lett.* **96** 073903
[3] Zhou X X, Xiao Z C, Luo H L and Wen S C 2012 *Phys. Rev. A* **85** 9335
[4] He S S, Zhou J X, Chen S Z, Shu W X, Luo H L and Wen S C 2020 *Opt. Lett.* **45** 877
[5] Cheng J, Wang G J, Dong P, Liu D P, Chi F F and Liu S L 2022 *Chin. Phys. B* **31** 014205
[6] Cao Y, Sheng L J, Cheng J H, Mei W and Ling X H 2024 *Opt. Laser Technol.* **174** 110583
[7] Wang L S, Zhou J X, Zeng K M, Chen S Z, Ling X H, Shu W X, Luo H L and Wen S C 2022 *APL Photon.* **5** 016105
[8] Ahlawat L, Kishor K and Sinha R K 2024 *Opt. Laser Technol.* **170** 110183
[9] Dong P, Xiang Y J and Cheng J 2023 *Ann. Phys.* (Berlin) **536** 2300351
[10] Zhou X X, Sheng L J and Ling X H 2018 *Sci. Rep.* **8** 1221
[11] Cheng J, Xiang Y J, Xu J H, Liu S L and Dong P 2022 *IEEE Sens. J.* **22** 12754
[12] Xiang Y J, Jiang X, You Q, Guo J and Dai X Y 2017 *Photon. Res.* **5** 467
[13] Tan X J and Zhu X S 2016 *Opt. Lett.* **41** 2478
[14] Jiang X, Wang Q K, Guo J, Chen S Q, Dai X Y and Xiang Y J 2018 *Plasmonics* **13** 1467
[15] Boltasseva A and Atwater H A 2011 *Science* **331** 290
[16] Zhong Y, Malagari S D, Hamilton T and Wasserman D M 2015 *J. Nanophotonics* **9** 093791
[17] Law S, Adams D C, Taylor A M and Wasserman D 2012 *Opt. Express* **20** 12155
[18] Zhang X, Wang Y, Zhao X, Huang T, Zeng S W and Ping P S 2019 *IEEE Photon. J.* **11** 4800808
[19] Cheng J, Wang C L, Li Y M, Zhang Y L, Liu S L and Dong P 2024 *Chin. Phys. B* **33** 084201
[20] Xu Y, Bai P, Zhou X, Akimov Y, Png C E, Ang L K, Knoll W and Wu L 2019 *Adv. Opt. Mater.* **7** 1801433
[21] Kretschmann E and Raether H 1968 *Z. Naturforsch. A* **23** 2135
[22] Dong P, Xiang Y J, Li R Z, Wang C L, Cheng C and Cheng J 2023 *Ann. Phys.* **535** 2300309
[23] Zegadi R, Lorrain N, Meziani S, Dumeige Y, Bodiou L, Guendouz M, Zegadi A and Charrier J 2022 *Sensors* **22** 844
[24] Barnes N P and Piltch M S 1979 *J. Opt. Soc. Am.* **69** 178
[25] Neuner B, Korobkin D, Fietz C, Carole D, Ferro G and Shvets G 2019 *Opt. Lett.* **34** 2667
[26] Luo H, Zhou X, Shu W, Wen S C and Fan D Y 2011 *Phys. Rev. A* **84** 043806
[27] Ling X H, Luo H L, Tang M and Wen S C 2012 *Chin. Phys. Lett.* **29** 074209
[28] Liang C K, Wang G H, Deng D M and Zhang T T 2021 *Opt. Express* **29** 29481
[29] Sui J Y, Zou J H, Liao S Y, Li B X and Zhang H F 2023 *Appl. Phys. Lett.* **122** 231105
[30] Sui J Y, Zou J H, Liao S Y, Wan B F and Zhang H F 2024 *IEEE Trans. Instrum. Meas.* **73** 7000109
[31] Ha D T, Thuy D T, Hoa V T, Van T T T and Viet N A 2017 *J. Phys.: Conf. Ser.* **865** 012007
[32] Yang W F, Ang L K, Zhang W T, Han J G and Xu X 2023 *Opt. Express* **31** 27041
[33] Zhu J Q, Ruan B X, You Q, Wu L M, Cai H Z and Dai X Y 2018 *IEEE Photon. J.* **10** 5900909
[34] Yang W, Zhang W and Xu Y 2024 *Opt. Express* **32** 42429
[35] Ling X, Xiao W, Chen S, Zhou X, Luo H and Zhou L 2021 *Phys. Rev. A* **103** 033515